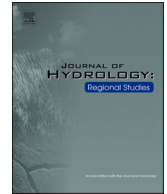




ELSEVIER

Contents lists available at ScienceDirect

Journal of Hydrology: Regional Studies

journal homepage: www.elsevier.com/locate/ejrh

Effect of climate change on soil erosion indicates a dominance of rainfall over LULC changes

Sushree Sangita Dash^a, Rajib Maity^{b,*,1}

^a School of Water Resources, Indian Institute of Technology Kharagpur, Kharagpur 721302, West Bengal, India

^b Department of Civil Engineering, Indian Institute of Technology Kharagpur, Kharagpur 721302, West Bengal, India

ARTICLE INFO

Keywords:

Soil erosion

Climate change

Rainfall

LULC

Revised universal soil loss equation (RUSLE)

Geographic information system (GIS)

ABSTRACT

Study region: Mahanadi River Basin in India

Study focus: This study explores the effect of climate change and human-induced farming and construction activities on soil erosion in a rainfed basin during two time periods viz. 1981–2000 and 2001–2019. This study assesses erosion using the Geographic Information System integrated Revised Universal Soil Loss Equation (GIS-integrated RUSLE) model. Three different analyses are designed to assess the effect i) combined effect of change in all the RUSLE factors over these two time periods, ii) effect of only land use/cover change (LULC), and iii) only rainfall change impact on erosion rate. A modified sediment delivery ratio (SDR) has been proposed and the model performances are validated using the observed Sediment Yield data.

New hydrological insights for the region: The results indicate an overall decrease in the erosion rate as a combined effect of change in all the factors, but at the same time, an increase in the spatial extent of the areas affected by soil erosion is noticed. The mean soil erosion rate varies between 37.02 tons ha⁻¹ yr⁻¹ in 1981–2000 and 31.89 tons ha⁻¹ yr⁻¹ in 2001–2019, with a 40% decrease in the maximum erosion rate, while the total and mean erosion rates are both down 13.85% compared to 1981–2000. The analysis suggested overall effect of the change in rainfall is more profound on erosion than LULC change.

1. Introduction

Climate change is defined as the change in climate conditions, such as long-term shifts in temperatures and weather patterns that continue to occur for a longer time, usually decades or more (IPCC, 2014). The rising temperature across the globe leads to an increase in the atmosphere's moisture content (Wang et al., 2021, 2022). Eventually, the regional weather circulation patterns are influenced by the elevating water vapor concentration in the atmosphere. It results in shifting of weather circulation patterns affecting the frequency, severity, and amount of heavy rainstorms throughout the year (Wang et al., 2017; Myhre et al., 2019).

In many regions throughout the world, climate change is predicted to affect soil erosion, which will have an impact on ecological systems and social well-being (Eekhout and de Vente, 2022).

Soil erosion, in general, is a detrimental hydro-geological phenomenon that leads to a loss of soil fertility due to the degradation of plant nutrients in surface soil and promotes water pollution by increasing sedimentation. It involves the detachment, transportation,

* Corresponding author.

E-mail address: rajib@civil.iitkgp.ac.in (R. Maity).

¹ ORCID: 0000-0001-5631-9553

<https://doi.org/10.1016/j.ejrh.2023.101373>

Received 3 May 2022; Received in revised form 30 March 2023; Accepted 31 March 2023

Available online 5 April 2023

2214-5818/© 2023 The Author(s). Published by Elsevier B.V. This is an open access article under the CC BY-NC-ND license (<http://creativecommons.org/licenses/by-nc-nd/4.0/>).

and deposition of particles of soil transferred from place to place. According to the FAO-led Global Soil Partnership, 75 billion tonnes (Pg) of soil are lost annually from agricultural areas around the world, resulting in an economic loss of US\$400 billion each year (Borrelli et al., 2017).

During the soil erosion phenomenon, water plays a vital role, which is exacerbated by anthropogenic activities almost worldwide (Gabriels and Cornelis, 2009). Specifically, the change in climate and Land Use Land Cover (LULC) through extreme hydrological cycles are one of the leading causes of soil erosion (Borrelli et al., 2020). It affects a range of physiochemical soil characteristics that drive infiltration and erosion mechanisms. Most of the previous studies over worldwide provided valuable information about soil erosion in the context of climate change, e.g., rainfall erosivity is examined for various climate models and scenarios adopted by the Intergovernmental Panel on Climate Change (IPCC), while other factors such as LULC are held constant (Chakraborty et al., 2020; Pal, Chakraborty, 2019; Gupta and Kumar, 2017; Khare et al., 2017; Doulabian et al., 2021), in context of both climate and LULC change (Op de Hipt et al., 2019; dos Santos et al., 2021; Belay and Mengistu, 2021; Pal et al., 2021) to observe changes in erosion using various models, taking spatiotemporal variability into account.

Although several studies have been done on the coupled and individual effects of climate and LULC variations on soil erosion, the background is still not fully grasped in terms of comparing variations in erosion rate by varying specific RUSLE model factors such as rainfall erosivity (*R*), crop management (*C*), conservation practice (*P*) while retaining other factors constant. To show the variations of climate change and LULC change, the studies have used various models including SHETRAN (de Hipt et al., 2019), SWAT (dos Santos et al., 2021), USLE (Mondal et al., 2015) and RUSLE (Belay and Mengistu, 2021). Only a few studies have considered the changes in land use and vegetation growth along with the effects of climate change on soil erosion because of the complexity (e.g., cultural, socioeconomic, ecological and political) (Li and Fang, 2016). Considering, the variation in LULC, leading to a change in *P* factor, changes in rainfall reflecting the change in *R* factor, change in NDVI (normalized difference vegetation index) resulting in a change in *C* factor, *K* (soil erodibility) and *LS* (Slope Length and Steepness), the RUSLE model can efficiently show the effect of land use pattern and, the erosive power of rainfall on the erosion rate. As a result, it is essential to decouple the effects of rainfall and LULC change in order to understand if there is any individual effect over a specific region.

Many earlier studies have verified the effectiveness of various erosion-quantifying physical models (Liu et al., 2006; Wu and Chen, 2012). But in order to drive the physical models, enormous amounts of data are needed, which is difficult and problematic for studies that take place over a lengthy period of time over a larger area (Borrelli et al., 2017).

Among all the empirical models, the Revised Universal Soil Loss Equation (RUSLE) is known for its versatility in field

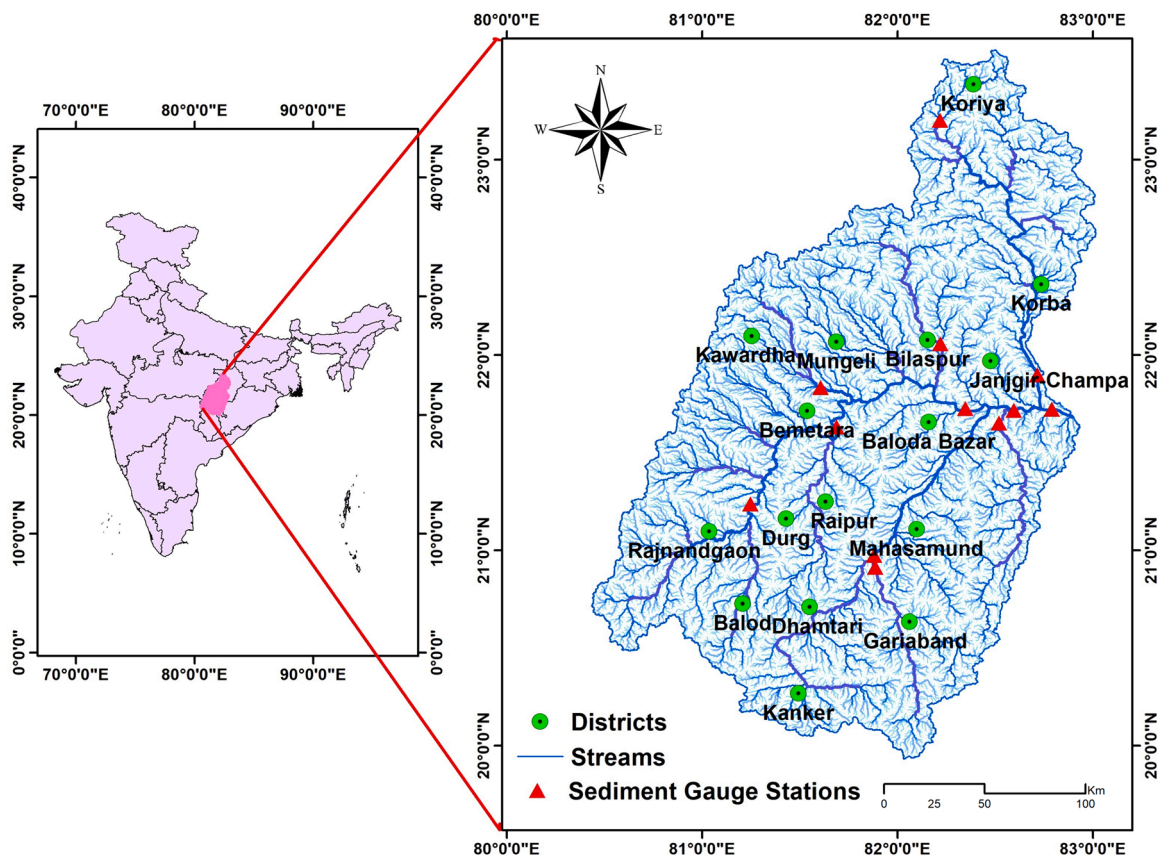


Fig. 1. Study area showing major stream network, districts and sediment gauge stations within the basin.

implementations and for being a standard tool for the adoption of conservational planning (Mahala, 2018). In India, runoff and soil loss data are limited and are usually obtained from gauging stations only (Patil et al., 2008). However, soil loss in ungauged watersheds needs to be determined accurately which is strenuous to quantify because the variables included in the erosion mechanism are complex. For the same, remote sensing (RS) and geographic information system (GIS) are highly effective techniques for studying soil erosion (Jena et al., 2018; Gupta and Kumar, 2017). The RUSLE model integrated with RS and GIS techniques provides user-friendly tool for identifying, quantifying, and mapping spatial distribution and prioritizing soil erosion-prone areas efficiently and affordably, which helps with improved planning and conservation activities (Eniyew et al., 2021).

Thus, the study aims to evaluate the soil erosion for two successive time periods, viz., 1981–2000 and 2001–2019 in the light of changing rainfall and LULC change by alternately varying various factors and keeping a particular factor constant for a control time period, i.e., 1981–2000, to assess the erosion causing factors and resulting sedimentation towards downstream regions.

Towards this, RS and GIS are integrated with the RUSLE model for basin-scale soil erosion assessment, and a rain-fed river basin, namely the upper part of the Mahanadi basin, being susceptible to water erosion, is considered as the study basin. There is a change in climate shift towards the end of the 20th century (around the 2000 s) (Houghton et al., 2001; Swanson et al., 2009; Wuebbles, 2018). Thus, the temporal length of this study has been divided into two periods to assess the effect of this remarkable climate change on soil erosion. The model outputs are validated using Sediment Delivery Ratio (SDR) approach. The approach can be used in other areas where observational data is scarce.

2. Materials and methods

2.1. Study area

The upper Mahanadi River basin covering the northeastern Deccan plateau area of the Mahanadi River basin between the latitude of 20.16°N and 22.75°N and longitude of 80.5°E and 82.5°E is selected for this study (Fig. 1). The Mahanadi River is India's seventh largest river, and it flows from west to east. It is draining a total coverage of 141,600 sq. km representing 4.30% of India's entire geological area (Pichuka and Maity, 2017; Asokan and Dutta, 2008). The total basin area of the upper Mahanadi basin is 58,711 sq. km with a perimeter of 2287 km including sixteen districts. The important crops cultivated in the region include rice, groundnut, sugarcane, millets, and vegetables. The average maximum temperature is 39.56 °C, while the average lowest temperature is 20.01 °C. The average highest relative humidity in the basin is 82% and the average lowest relative humidity is 31.6% (Water year Book, CWC, 2014). The basin is located in the agro-climatic area of the Eastern Plateau and Hills (Water year Book, CWC, 2014). The morphology of the Mahanadi upper sub-basin varies, with the dominating mountainous terrain in the northern upper section having elevations ranging from 196 to 1136 m. Agricultural land covers the majority of the basin, accounting for more than half of the total basin area. Soil texture in the study area is categorized as chromic vertisols, ferric luvisols, lithosols, and chromic luvisols. Ferric luvisols account for a large proportion of the basin, being prone to water erosion, as it has medium to low tolerance to yield reduction and is moderately susceptible to degradation (Stocking and Murnaghan, 2013). The assessment of soil erosion is important for the basin, given the physiographic and socio-economic characteristics of the basin.

2.2. Description of data used

Digital Elevation Model (DEM), Land Use Land Cover (LULC) map, rainfall data, Normalized Difference Vegetation Index (NDVI) map, and soil characteristics, such as sand, silt, and clay content and organic matter, are essential for the RUSLE model.

Daily rainfall data with a spatial resolution of 0.25° × 0.25° is obtained from India Meteorological Department (IMD) for 1981–2019. The entire length of data is divided into approximately two halves: 1981–2000 and 2001–2019, to assess the spatio-temporal variation in soil loss, considering the pre-2000 period as the base period.

The soil characteristics, i.e., percentages of sand, silt, clay, and organic carbon content, are obtained from Harmonized World Soil Database (HWSD), version 1.2, with 30 arcs spatial resolution (~900 m), available at the Food and Agriculture Organization of the United Nations.

The DEM of the study area with a 30 m spatial resolution is obtained Shuttle Radar Topography Mission (SRTM). It is used in the computation of topographic parameters, such as slope length and steepness factor.

The calculation of the Normalized Difference Vegetation Index (NDVI) map and the supervised classification of land use/land cover (LULC) map are carried out using Landsat 5 satellite imageries for the years 1985, 1990, and 2010 and Landsat 8 imagery for the year 2015.

Image processing is carried out by Google Earth Engine (GEE), and ArcGIS (version 10.3) is used for developing spatial maps of various input variables of the RUSLE model. Since prior to the 1990 s, Landsat imageries did not cover the entire study area, and significant changes are seen over a 5-year period following the 1990 s. Therefore, we considered 1990, 1995, 2010 and 2015 for the calculation of NDVI and for the preparation of LULC map. The calculation of median NDVI and supervised classification of LULC for the years 1985, 1990, 2010, and 2015 is carried out using the GEE.

The sediment yield data for two-time frames are collected from the Central Water Commission (CWC) sediment concentration measuring stations of the upper Mahanadi basin, extracted from the hydro-meteorological water yearbook of CWC. The different sediment gauge stations along the upper Mahanadi basin are shown in Fig. 1.

2.3. Model description

The RUSLE model is used for the assessment of soil erosion. It simplifies the complex physical mechanism for the long-term rate of soil erosion over an extensive area while retaining the main factors affecting the mechanism. For the forest and agricultural watersheds, RUSLE has been extensively employed to evaluate annual average soil erosion through enhanced methods to compute the soil erosion parameters (Renard et al., 1996). It is currently the most known modeling tool for simulating actual soil potential from coarser to finer spatial scales (Behera et al., 2020). According to Renard et al. (1996), the RUSLE factors are computed using rainfall, LULC, topography, and soil data. After that, the dynamics of streamflow and soil erosion can be assessed using a direct correlation between rainfall and runoff. This approach is broadly adopted to evaluate the soil loss, and therefore, its hazard assessment guides in rehabilitating the areas prone to erosion by adopting appropriate management policies (Biswas and Pani, 2015; Ostovari et al., 2017).

2.4. RUSLE model parameterization

The RUSLE model comprises five input factors to compute the mean annual soil erosion in a region. The formulation is expressed as:

$$A = R \times K \times LS \times C \times P \quad (1)$$

where K indicates the soil erodibility factor ($\text{ton ha}^{-1}\text{MJ}^{-1}\text{mm}^{-1}$), R indicates the rainfall erosivity factor ($\text{MJ mm ha}^{-1} \text{h}^{-1} \text{yr}^{-1}$), LS indicates the topographic factor (dimensionless), P is the conservation practice factor (dimensionless) (0–1), C indicates the cover management factor (dimensionless) (0–1.5), A indicates the mean annual potential soil loss ($\text{tons ha}^{-1} \text{yr}^{-1}$). All these factors are discussed one by one.

2.4.1. Rainfall erosivity factor

Rainfall erosivity factor (R) is the potential of rainfall to separate the soil particles from the soil layer. It is the measure of the erosive strength of rainfall. It depends on the intensity, duration, and volume of the precipitation and it can be calculated as a specific rainstorm or sequence of rainstorms to calculate erosivity cumulatively. The most common type of erosion in barren land is splash erosion. The value of R factor is computed from Eq. (2). It was originally developed by Wischmeier and Smith (1978) to establish the relation between rainfall depth and rainfall erosivity and afterward amended by Arnoldus (1980) for the inclusion of monthly rainfall dynamics.

$$R = \sum_{i=1}^{12} 1.735 \times 10^{\left(1.5 \times \log \left(\frac{P_i^2}{P} \right) - 0.08188 \right)} \quad (2)$$

where P is the average annual rainfall magnitude (mm), P_i is the rainfall of i^{th} month (mm), R is an average rainfall erosivity factor ($\text{MJ mm ha}^{-1}\text{h}^{-1} \text{yr}^{-1}$).

2.4.2. Soil erodibility factor

Soil erodibility factor (K) is the vulnerability of the top layer of soil to erosion, sediment transport capacity, and runoff rates under standard conditions. It is measured as the soil loss on a 22.13 m long plot with 9% slope, kept in constant fallow, tilled along the slope of a hill (Weesies et al., 1998). The K factor value is calculated by adopting the Eq. (3) given by Wischmeier and Smith (1978).

$$K = \frac{1.2917(2.1 \times 10^{-4} \times M^{1.14}(12 - \text{OM}) \times 3.25 \times (S - 2) + 2.5 \times (\rho - 3))}{100} \quad (3)$$

where OM refers to the % of organic matter content in the soil; S indicates the value corresponding to structural classes (1 for very fine granular; 2 for fine granular; 3 for medium or coarse granular and 4 for blocky, platy or massive structure); ρ indicates the value corresponding to the permeability class (1 for rapid; 2 for moderate to rapid; 3 for moderate; 4 for slow to moderate; 5 for slow and 6 for very slow permeability rate); and M is a function of soil primary particle size fraction given by: $M = (\% \text{ of silt} + \% \text{ of very fine sand}) \times (100 - \% \text{ of clay})$. The study area has three types of soil with different soil characteristics as used in Eq. (3).

2.4.3. Topographic factor

The slope length and steepness, collectively called the topographic factor (LS), is the linear distance joining the beginning of the overland flow and the point where slope length lowers for the deposition process. The equation for evaluating the LS factor in the RUSLE model considers rill erosion, unlike the USLE model. In specific, the moving process of the erosion mechanism is controlled mainly by the topographical factor. The LS factor is computed from Eq. (4) (Mitasova and Mitas, 2001):

$$LS = \left(FA \times \frac{CS}{22.13} \right)^{0.4} \times \left(\frac{\text{Sin}\theta}{0.0896} \right)^{1.3} \quad (4)$$

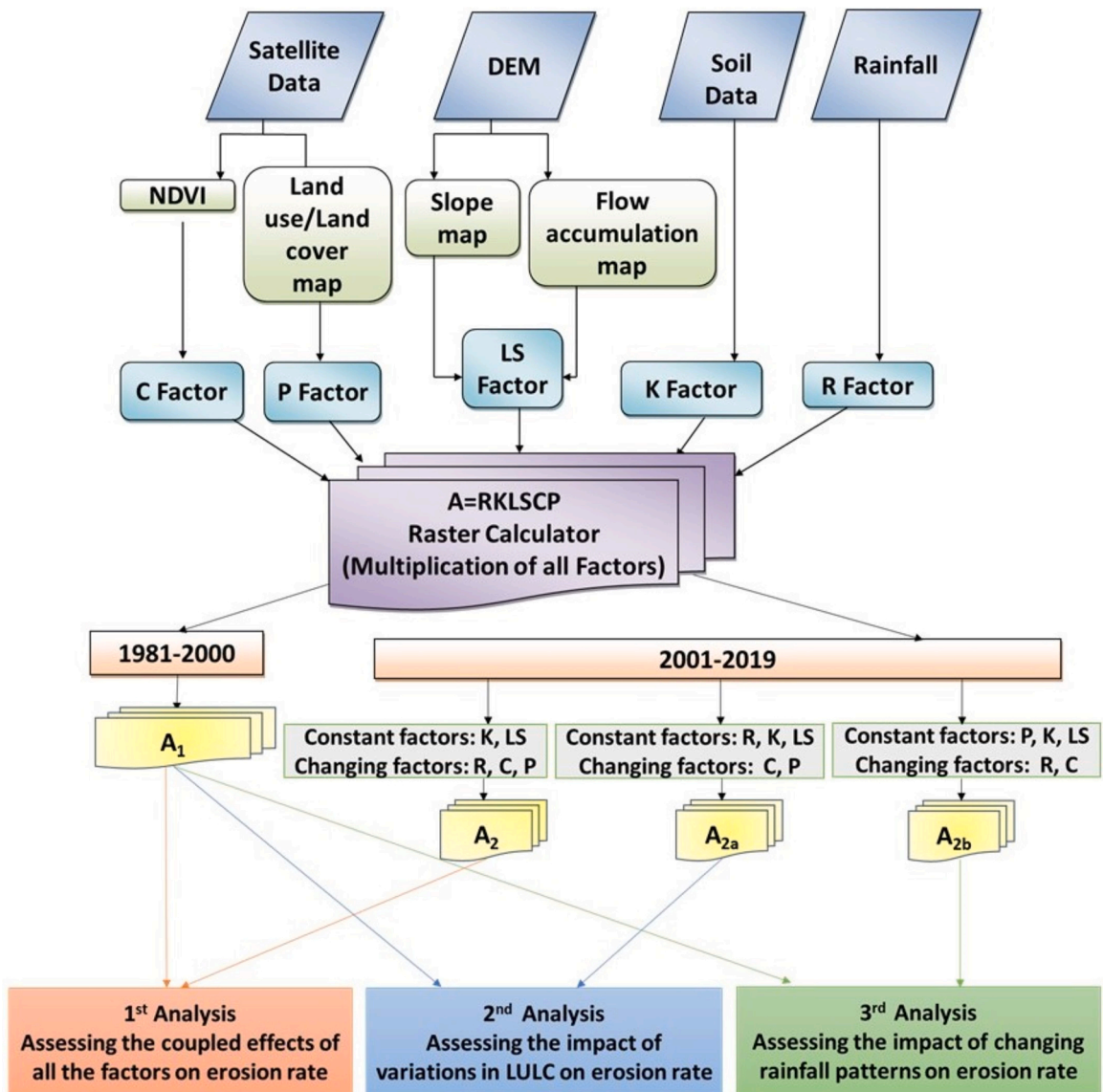
where FA is the flow accumulation and CS is the cell size of the DEM data (in our case, 30 m), θ is the slope angle of the drainage basin (in degrees).

2.4.4. Cover management factor

The cover management factor (*C*) is the ratio of soil loss from cultivated land to relative soil loss from continuous, clean tilled fallow land in specific conditions. Several researchers allocated the *C* factor on the basis of LULC. However, the changes in vegetation cover and density were not included in these analyses. Therefore, in this analysis, Normalized Difference Vegetation Index (*NDVI*) is used to consider variability between scrubland and forests. To calculate the *NDVI* for every pixel in the study area, Eq. (5) is used (Jena et al., 2018).

$$NDVI = \frac{(NIR - Red)}{(NIR + Red)} \tag{5}$$

where *NIR* and *Red* are the measures of spectral reflectance obtained in the near-infrared and visible spectrum, respectively. The value of *NDVI* lies between - 1 and + 1. Within the near-infrared part of the electromagnetic spectrum, the photosynthetically active vegetation exhibits high reflectivity as compared to the *Red* portion. Therefore, very high values of *NDVI* are observed for active



A1 and A2 are the soil loss when all the factors are changing except K and LS factor in 1981-2000 and 2001-2019, respectively; A2a is the soil loss when C and P factor are changing while R,K and LS factor are constant during 2001-2019; A2b is the soil loss when R and C factor are changing while P, K, LS factor are constant during 2001-2019

Fig. 2. Data requirement and technical flowchart for the study using RUSLE model.

photosynthesis vegetation. The C factor is computed from Eq. (6) (Durigon et al., 2014).

$$C = e^{\frac{-2NDVI}{1-NDVI}} \quad (6)$$

2.4.5. Support practice factor

The support practice (P) is the ratio between soil loss through a particular management practice to the relative loss with up and downslope plowing (Renard et al., 1996). The P factor in the current study is allocated in accordance with the management practices for different LULC as represented in Table S1 in Supplementary Material. The value varies between 0 and 1, with the highest value for land without management practice and the lowest value for land with management practices.

2.5. Climate change effect analysis

The most severe environmental alteration is expected as a consequence of climate change (Perović et al., 2019). The soil erosion quantification is subject to vary in the perspective of climate change in response to changes in rainfall, vegetation indices, and LULC over time periods. The magnitude and intensity of rainfall directly affect the RUSLE model. As a result, a modified evaluation of the Rainfall erosivity (R) factor for different time periods is inevitable under the climate change aspect. In this regard, the R factors for two time periods, 1981–2000 and 2001–2019, are determined.

The most significant connection among the soil, soil moisture, and the atmosphere is the vegetation (Chuai et al., 2013). Seasonal as well as annual climate variations affect natural vegetation (Bagherzadeh et al., 2020; Zhang et al., 2011; Cui and Shi, 2010). In this study, the NDVI for the years 1990 and 1995 are calculated and the spatial map for both years are averaged using raster calculator in the ArcGIS environment to prepare a spatially distributed NDVI map for the time frame 1981–2000. Similarly, the spatially distributed NDVI map for the years 2010 and 2015 are averaged to account for soil loss estimation for the period of 2001–2019.

Change in land productivity that contributes to LULC change is also a crucial aspect to assess soil erosion. Land use planning and ecological growth need a thorough knowledge of the spatiotemporal variation of soil erosion on account of LULC change (Keesstra et al., 2016). The spatially distributed LULC map for both the time periods, viz. 1981–2000 and 2001–2019 are computed by calculating the average of the spatially distributed LULC map of 1990 and 1995 for the time period 1981–2000 and the LULC maps of 2010 and 2015 are used to prepare the LULC map for the time frame 2001–2019. The average map is prepared using the raster calculator in the ArcGIS environment. Furthermore, the topographic factor, soil type, and soil texture are subject to very slow alterations over the years (Behera et al., 2020). Thus, the soil erodibility factor (K), a function of soil type, and the topographic factor (LS), a function of slope length and steepness, are considered as constant in this study.

In this study, three analyses are performed keeping the K factor and LS factor as constant in all the analyses to delineate the effects of other factors related to climate and terrestrial conditions on soil erosion. Firstly, the coupled effects of three changing factors, viz. the R factor, C factor and P factor on erosion rate are observed by updating all the three factors for the time periods of analysis (pre-and post-2000). Subsequently, the individual effects of change in rainfall and LULC over time are analyzed. For that, in the second analysis, the influence of LULC variations on erosion rate is assessed by considering 1981–2000 as the control period, varying C and P factors and assuming the R factor as constant throughout the time. In the last analysis, the influence of changing rainfall on erosion is assessed by taking the P factor as constant over time, while the C factor and R factor are varied by anticipating 1981–2000 as the control period.

Using the methodology discussed for calculating C factor, R factor, and P factor, different maps are prepared for both time periods of 1981–2000 and 2001–2019. Furthermore, these factors are multiplied with K factor and LS factor in developing a potential soil erosion map intended for respective time periods. The operational flow chart of the overall methodological approach is shown in Fig. 2.

2.6. Validation using sediment yield data

When soil erodes, a portion of it is moved through the channel section and makes a significant contribution to sediment yield, whereas the remaining portion is stored in the channel. Multiple soil erosion and sedimentation studies have been conducted to analyze the relationship between soil loss inside a drainage basin and Sediment Yield (SY) at the outlet point. The Sediment Delivery Ratio (SDR), a lumped concept, can be used to calculate the SY . The SDR is defined as the ratio of sediment yield calculated at a channel point to gross highlands soil erosion, including sheet, rill, gully, and channel erosion. However, the RUSLE only estimates rill and interrill or sheet erosion, which is regarded as a significant contributing factor to gross erosion. This concept of SDR takes into account a number of processes that occur throughout on-site soil erosion and the sediment yield at the outlet (Van Rompaey et al., 2001). A variety of factors can influence SDR , including channel density, sediment source, proximity to the mainstream, texture, basin area, length, slope, rainfall-runoff factors, and land use/land cover. The SDR of a watershed with steep slopes is greater than that of a watershed with flat and broad valleys. In general, the lesser the SDR , the greater the area size. Several SDR models have been developed and utilized to determine SY as tabulated in Table S5 in Supplementary Material. However, the selection of the best SDR model for a certain basin is cumbersome, owing to the lack of studies involving this technique using observational data. The drainage area method as given in Eq. (7) is the most commonly and widely used method for estimating SDR (De Vente et al., 2007).

$$SDR = a \times D^{-b} \quad (7)$$

where D is the drainage basin area (in km^2); and a and b are correction factors related to the physical characteristics of the basin. The adjustment b variable has a negative sign as it signifies that with an increase in the basin area, the SDR decreases. The various SDR

models extensively used in the literature are provided in Table S2 in Supplementary Material. In this study, we have used observed sediment yield values obtained from CWC's sediment concentration measuring stations in the study basin. The average SY data is collected from 1981 to 2019. The average SY for the periods is calculated for twelve sub-basins of the study basin, namely, Andhiyarkore, Bamnidih, Baronda, Basantpur, Ghatora, Jondhra, Kotni, Manendragarh, Rajim, Rampur, Seorinarayan and Simga having sediment gauging station (Fig. 1) for the periods 1981–2000 and 2001–2019. Using these data, the parameters in Eq. (7) are calibrated for the study basin as discussed later in Results and Discussion section. Finally, the estimated sediment yield (SY_{est}) is evaluated as follows:

$$SY_{est} = SDR \times GSL \quad (8)$$

where GSL is the gross soil loss and both SY_{est} and GSL are in tons.yr^{-1} .

3. Results and discussion

The spatial variation of mean annual precipitation for two successive periods 1981–2000 and 2001–2019 is shown in Fig. S1a and Fig. S2b, respectively in Supplementary Material. It is observed that average rainfall per year differs from 915 mm to 1623 mm, with the maximum value confined to the northern part of the basin during the years 1981–2000 and from 960 mm to 1414 mm with the maximum value found in the southern and most of the northern areas of the basin during 2001–2019. The rainfall erosivity factor (R), as shown in Fig. S1c and S1d in supplementary material ranges between 2029 and 8168 $\text{MJ mm ha}^{-1} \text{h}^{-1} \text{yr}^{-1}$ during 1981–2000 and from 40 to 4609 $\text{MJ mm ha}^{-1} \text{h}^{-1} \text{yr}^{-1}$ during 2001–2019. It is noticed that the northwestern part of the basin, such as the Kawardha and Mungeli districts, having low R factor during 1981–2000, is found to have a slight increase in R factor during 2001–2019. On the other hand, the central part of the basin, such as Bemetara, Baloda Bazar, Raipur, and Mahasmond, is found to have more drastic increase in R factor during 2001–2019. The southeastern part of the basin spanning over the Gariaband and Kanker districts having medium R factor during 1981–2000 exhibits more R factor during 2001–2019. Similarly, the southern part of the basin (Balod, Dhamatari and Durg districts) is characterized by medium R factor during 1981–2000 that reduces during 2001–2019. The rest of the basin area is noticed to have more or less steady R factor for the considered time periods. It is observed that the higher R factor is spatially distributed over northern and southwestern regions during 1981–2000, and over northern and eastern parts during 2001–2019. This may be the result of erratic rainfall across the study area and the similar phenomena were also reported for Huaihe River Basin, China by Wei et al. (2022) and Yangtze River basin, China by Huang et al. (2013). Peng et al. (2022) suggested that the rise in rainfall intensity would result in higher erosion rates. Soil erodibility is a measurement of a soil's cohesive character, which is governed by the physical and chemical characteristics of soil and thus influencing its erodibility potential. The spatially distributed K factor map is illustrated in Fig. S2a in Supplementary Material. The K factor varies as, 0.043 $\text{tons h MJ}^{-1} \text{mm}^{-1}$ for clay soil, 0.065 $\text{ton h MJ}^{-1} \text{mm}^{-1}$ for loam soil, 0.069 $\text{ton h MJ}^{-1} \text{mm}^{-1}$ for sandy clay loam soil, and 0.075 $\text{ton h MJ}^{-1} \text{mm}^{-1}$ for sandy loam soil. It is noticed that a large part of the basin is covered by sandy loam soil with a maximum K factor value. Lower K values are found for clay soil covering the least part (i.e., 0.029%) of the study area. In clay soil, the higher percentage of clay than sand has a more cohesive nature that binds the soil particles, thus reducing its susceptibility to erosion.

The topographic factor defines the impact of slope steepness (S) and slope length (L) factors on soil erosion. The results represented in Fig. S2b in Supplementary Material shows that 94.25% of the watershed has LS value < 5 , indicating a less varied topography of the basin. Correspondingly, 3.09%, 2.09%, 0.37%, 0.07%, and 0.09% of the basin have LS value in the range of 5–10, 10–25, 25–50, 50–75, and > 75 , respectively (Table S2 in Supplementary Material).

NDVI is calculated to measure the C factor. The NDVI gives more detail regarding the density and condition of the vegetation cover. It better represents the spatial variation of the factor C for the two successive years, as illustrated in Fig. S3 in Supplementary Material. Low C factor values are associated with dense forests, while high values are associated with fallow lands and crop fields as observed from the results. The percentage of area covered under each class of C factor for two successive periods is compared in Table S3 in Supplementary Material. The C factor value ranging from 0.3 to 0.5 accounted for 88.39% of the study area during 1981–2000 that increased to 89.02% during 2001–2019. As soil surfaces are considered vulnerable to bare soil and pastureland, a higher value of the C factor indicates more susceptibility to soil erosion (Dash et al., 2021). Therefore, the higher range for the C factor of 0.7–1 implies increased soil erosion susceptibility since they are assessed as exposed soil surfaces. It is depicted that an insignificant rise in the area coverage made up 0.001% (1981–2000) to 0.007% (2001–2019) for the C factor value of 0.7–1. However, a decline is elucidated for the area coverage for the C factor value of 0–0.1, 0.1–0.3, 0.5–0.7 from 1981 to 2000–2000–2019. The C factor value of 0.1–0.3 is found to be decreased for some northwestern, southwestern and central parts of the basin, covering the districts such as Rajnandgaon, Kawardha, Bemetara, and Bilaspur, whereas it is found to be increased in the northeastern, southeastern and southern parts of the basin including districts like Korba, Dhamatari, Gariaband, and Mahasmond during 2001–2019. The decline in C factor values in some parts of the area over the years suggests a decrement in soil erosion rate.

The P factor denotes the decreased soil erosion threat caused by supportive management structures implemented in a particular area. Its value is allocated based on various LULC classes. The average of the LULC map for the years 1990 and 1995 (Fig. S4a in Supplementary Material) is considered to evaluate the P factor for the time period of 1981–2000 (Fig. S4c in Supplementary Material). Likewise, the average of the LULC map for the years 2010 and 2015 (Fig. S4b in Supplementary Material) is considered to evaluate the P factor for the time period of 2001–2019 (Fig. S4d in Supplementary Material). It is found that the maximum part of the basin is covered by agricultural cropland. Table S4 in Supplementary Material depicts the areal distribution for the LULC over two successive periods. It is observed that there is a decline in forest cover (25.5–22.93%) and fallow land (28.95–22.22%) from 1981 to

2000–2001–2019. However, there is an increase in water bodies (0.55–0.96%), agricultural cropland (35.84–39.05%), built-up (1.38–4.94%), and barren land (7.78–9.9%) over the years. This shows that most of the study area is affected by climate change. The *P* factor value ranges from 0 to 1. The maximum value for *P* factor in 1981–2000 is found to be surrounding some parts of the northern, southern and eastern basin area (Koriya, Manendragarh, Kanker, Mahasamund, and Baloda Bazar) that has been decreased during 2001–2019. However, the area of the basin covering the northwestern part of the basin (Kawardha and Mungeli) shows an increase in *P* factor value for the year 2001–2019 than in 1980–2000. Considering the outcomes of all the RUSLE factors for both the time periods, i.e., 1981–2000 and 2001–2019, three further analyses are carried out.

The factors so prepared in raster map form are multiplied in the raster calculator in ArcGIS 10.3 system to obtain spatially distributed erosion map. The spatially distributed maps of soil erosion are reclassified into eight erosion classes by following the consumer-specified classification criterion. The erosion classes, along with the percentage of areal coverage for all three analyses, are provided in Table 1. The average annual potential soil erosion varying pixel-wise across the upper Mahanadi basin for all three analyses are depicted in Fig. S5 in Supplementary Material.

Overall, in all three analyses, the erosion rate including the maximum, mean and total erosion rate are observed to be reduced during 2001–2019 than during 1981–2000 period as depicted in Table 2. In the first analysis, the average annual soil erosion is estimated concerning the coupled effect of factors such as conservation practice (*P*) factor, crop management (*C*) factor, and rainfall erosivity (*R*) factor keeping other factors, namely topographic (*LS*) factor and erodibility (*K*) factor constant over the years. From the study, it is found that the mean soil erosion rate varies as 37.02 ton ha⁻¹ yr⁻¹ in 1981–2000 and 31.89 ton ha⁻¹ yr⁻¹ in 2001–2019, with a decrement of maximum rate from 2.5×10^5 ton ha⁻¹ yr⁻¹ (1981–2000) to 1.5×10^5 ton ha⁻¹ yr⁻¹ (2001–2019). The total erosion rate is about 217.35-million-ton yr⁻¹ (1981–2000) and 187.23 million ton yr⁻¹ (2001–2019). The maximum erosion rate is decreased by 40%, whereas the total and mean erosion rate is decreased by and 13.85% with respect to 1981–2000.

It is observed that, there is a gradual decline in soil erosion seen in the northern and eastern parts of the basin over the years. The region with the greatest percentage drop is found to be laid out with vegetation with a decline in rainfall over the years and are having reduced slope. The maximum soil erosion for both the time periods is found at the northern part of the basin, i.e., at Chirimiri, the largest city and a hill station with steep slopes of the Manendragarh district of Chhattisgarh (Fig. S5 in Supplementary Material). Furthermore, Habtu and Jayappa (2022) confirmed that the north and northeastern sections of their study region with hilly and mountainous topography have a moderate to extremely severe erosion vulnerability due to steep slopes and high rainfall.

From the reclassified erosion map, it is found that the area under the negligible erosion group (5–10 tons ha⁻¹ yr⁻¹) covers the maximum part of the basin, while the least area is under severe erosion for both time periods. Nonetheless, it covers 67.4% of the area during 1981–2000, which climbs up to 71.5% during 2001–2019. This shows that it is highly likely for those places to face increased soil erosion hazards in the future. However, the rest of the reclassified erosion rates (Table 5) are observed to decline over the years for that basin area. This is attributed to the increasing spatial coverage of the study region as corroborated by other works (Allafta and Opp, 2022; Habtu and Jayappa, 2022). Besides, this could be due to change in rainfall, change in crop management practices, and LULC over the periods. Since rainfall acts as a vital contributor to the soil erosion processes, climate change is likely to affect soil erosion through changes in rainfall (Mondal et al., 2015). Soil erosion may be increased or decreased as a result of LULC changes. Changes in LULC (i.e., the spread of cultivated area) lead to increased soil erosion, which is expected to intensify with increased precipitation (Belay and Mengistu, 2021).

The areal extent in terms of percentage for the change in erosion rate for the three analyses are illustrated in Table 3. The change in erosion rate along with the areal coverage for each categorized change rate for all three analyses is shown in Fig. 3. For the first analysis, almost 83% area of the study region exhibits a reduced change in the erosion rate during 2001–2019 as compared to the past time frame, i.e., 1981–2000. Nearly 19% area shows a negative change in erosion rate mostly across the northern and southern parts, wherein for 64% of the entire study area, the reduction lies in the range of -5 – 0 tons ha⁻¹ yr⁻¹. It is found that the *R* and *C* factor declines during 2001–2019 prior to 1981–2000. Moreover, during 2001–2019, it is observed that there are more built-up areas and water bodies, less fallow land and forest areas influencing the *P* factor. All these factors (*R*, *C*, *P*) together represent the higher decline in erosion rate during 2001–2019 than 1981–2000. The rainfall erosivity factor (*R*) is an important factor that results in soil erosion (Wei et al., 2022). He et al. (2022) and Kabolizadeh et al. (2022) showed that the potential of erosion decreases along with the value of

Table 1

Percentage of basin area for different soil erosion class during 1981–2000 (control period) and 2001–2019 (according to three different analyses). Fig. 2 may be referred for the details of three analysis.

Soil Erosion Class	Erosion Range (ton ha ⁻¹ yr ⁻¹)	Percentage of study area covered (%)			
		Control Period	First Analysis	Second Analysis	Third Analysis
		1981–2000	2001–2019		
Negligible	0–5	67.4	71.50	71.59	67.48
Very low	5–10	4.44	4.04	4.13	4.40
Low	10–20	6.36	5.68	5.68	6.39
Slight	20–40	7.32	6.36	6.21	7.47
Moderate	40–80	6.63	5.66	5.52	6.76
High	80–160	4.32	3.65	3.67	4.19
Very High	160–320	2.03	1.75	1.79	1.87
Severe	> 320	1.5	1.36	1.39	1.39

Table 2
Maximum, mean and total erosion rate for all the three analyses during 1981–2000 and 2001–2019.

Analysis ^a	Assessment target	1981–2000			2001–2019		
		Maximum erosion rate (tons/ha/yr)	Mean erosion rate (tons/ha/yr)	Total erosion rate (Million tons/yr)	Maximum erosion rate (tons/ha/yr)	Mean erosion rate (tons/ha/yr)	Total erosion rate (Million tons/yr)
First Analysis	Assessing the coupled effects of all the factors on erosion rate	2.60×10^5	37.02	217.35	1.57×10^5	31.89	187.23
Second Analysis	Assessing the impact of variations in LULC on erosion rate	2.60×10^5	37.02	217.35	1.55×10^5	32.27	189.46
Third Analysis	Assessing the impact of changing rainfall shifts on erosion rate	2.60×10^5	37.02	217.35	1.90×10^5	35.23	206.83

^a Fig. 2 may be referred for the details of three analysis

Table 3

Percentage of basin area for the change in erosion rate for the three analyses. Fig. 2 may be referred for the details of three analysis.

Change in erosion rate (tons ha ⁻¹ yr ⁻¹)	Percentage of study area covered (%)		
	First Analysis	Second Analysis	Third Analysis
< -50	5.75	5.48	1.05
-50 to -25	3.79	3.47	1.33
-25 to -10	5.29	4.86	3.09
-10 to -5	3.21	3.25	2.88
-5-0	61.82	65.17	73.84
0-5	6.77	6.06	12
5-10	2.91	2.30	2.61
10 to- 25	3.98	3.24	2.08
> 25	6.44	6.13	1.06

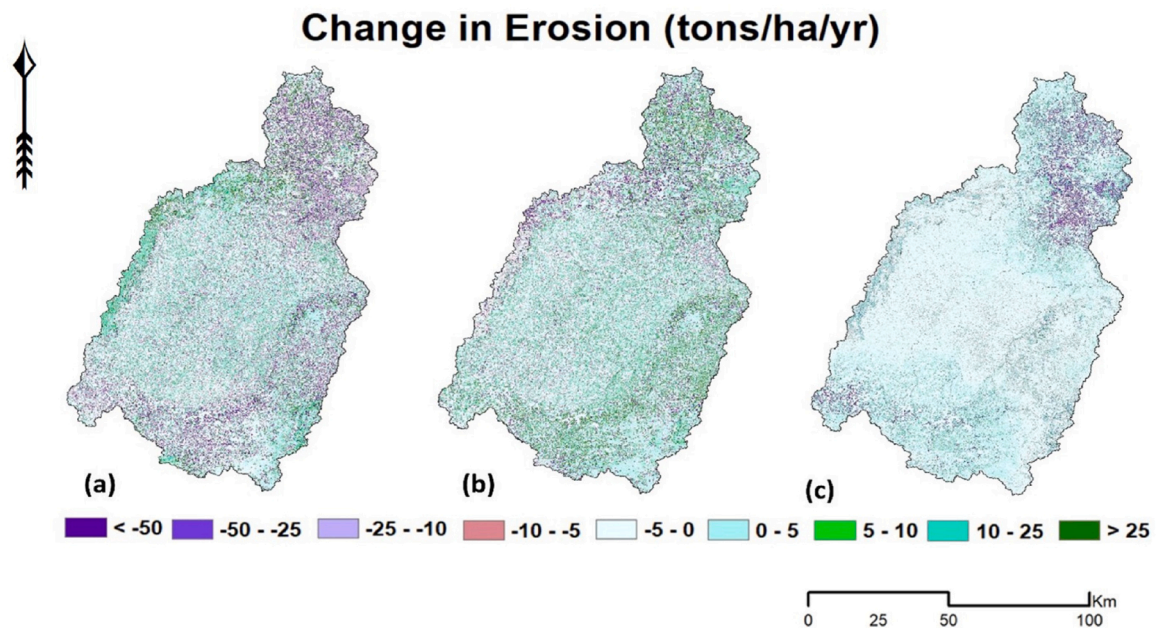


Fig. 3. Change in erosion rate (ton ha⁻¹ yr⁻¹) showing (a) coupled effects of both rainfall and LULC, (b) individual effect of LULC while holding rainfall variation as constant, and (c) individual effect of rainfall variation while holding LULC as constant.

rainfall erosivity (R) factor. An effective indicator of soil erosion is vegetation cover, it can gradually reduce overall soil loss by protecting the topsoil from the direct effects of precipitation (Novara et al., 2019). There has been an increase in vegetation cover during 2001–2019 than 1981–2000 that result in a decrease in the C factor and thus the erosion rate. Other studies (Kavian et al., 2019; Almohamad, 2020; Macedo et al., 2021; Kabolizadeh et al., 2022) have made reference to this, and the findings of this study are similar with those. For this study, the SDR approach is used for validating the outcomes of this research. Our findings revealed that SY levels are overestimated. The substantial inaccuracies could be due to observations that were made with probable uncertainty and/or model development uncertainty. Our findings regarding overestimation of sediment yield quite resembled to the study done on sediment yield modelling in Tawi River of Jammu region, India by Rawat et al. (2022). Due to the great complexity of the sediment delivery mechanism and the necessity to examine the interrelationship between their intervenient components to adapt the equation, it is difficult to develop a universal equation to estimate the SDR in a basin (Walling, 1983). On that account, we adjusted SDR equation by Vanoni (1975) accordingly to minimize the disparity between the estimated and observed sediment yield (SY_{obs} and SY_{est}) for our study area. The twelve sub-basins are divided into two-thirds for calibration and one-third for validation purposes. Thus, 3-fold cross-validation is used to obtain a more accurate and dependable coefficient of SDR for the study basin. The value of a from Eq. (7) is optimized, considering a wide range of values from 0.05 to 0.5. The optimum value of a is selected based on the least RMSE between SY_{obs} and SY_{est} and a reasonable difference between calibration and validation error across the folds and two time periods. Results of 3-fold cross-validation reveal that Eq. (9) is the best suited for predicting SDR for the study basin (D in km²).

$$SDR = 0.1 \times D^{-0.125} \quad (9)$$

The plot between the observed and predicted sediment yield data for both the time periods is represented in Fig. 4. The twelve

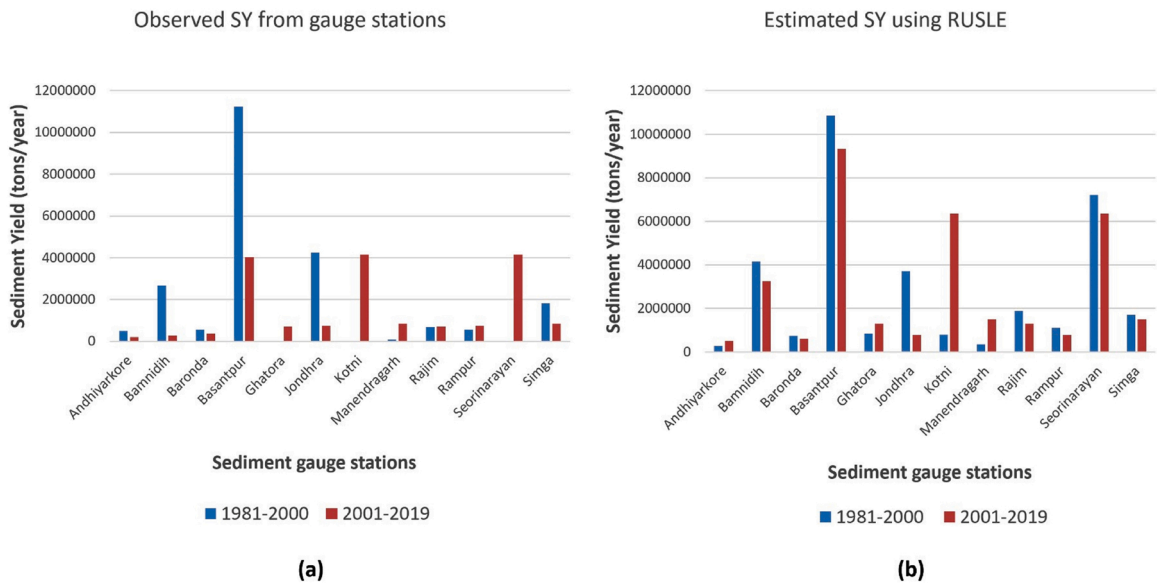


Fig. 4. Average sediment yield during 1981–2000 and 2001–2019: (a) observed SY from gauge station, and (b) estimated SY using RUSLE.

sediment gauge stations, along with their respective SDR, SY_{obs} and SY_{est} for both 1981–2000 and 2001–2019 time periods are represented in Table 4. Overall, it is observed that the gross soil erosion and the sediment yield over the basin reduces in 2001–2019 as compared to 1981–2000.

A Spearman’s rank correlation analysis was performed for average annual rainfall and average annual soil erosion for both period of datasets. During 1981–2000, soil erosion and rainfall were strongly positively correlated ($r = 0.525$, $p < 0.01$). While, during the period 2001–2019, soil erosion and rainfall were moderately correlated ($r = 0.160$, $p < 0.01$).

The preliminary correlation analysis suggests that the rainfall have a positive impact on the soil loss, while more detailed analysis is required to explore the full mechanism. Since, soil loss depends on the duration of rainfall, and more importantly rainfall intensity, the effect of rainfall frequency and intensity can show more positive correlation with erosion.

A Similar type of study on the comparison of rainfall and erosion has been done earlier by various researchers. Martínez-Mena et al. (2020) evaluated the effects of various sustainable management practices on erosion in two rainfed systems in Spain. They found that the Spearman’s correlation between rainfall erosivity and soil erosion was found to be 0.52 with $p < 0.01$ and they found that erosive responses were correlated much more closely with the rainfall intensity than with the rainfall depth. Huang et al. (2020) found that Spearman’s rank correlation analysis showed actual soil loss related to annual rainfall positively. Strong correlation was ($r \geq 0.7$) observed in more than 50% area and were statistically significant at 95% confidence level.

The second analysis shows the impact of variation in LULC (P factor) on erosion rate. The maximum, mean and total erosion rate are found to be 1.55×10^5 tons $ha^{-1} yr^{-1}$, 32.27 tons $ha^{-1} yr^{-1}$ and 189.46 million tons yr^{-1} , respectively. From the reclassified erosion map, as shown in Fig. S5 in Supplementary Material, it is found that the area under each erosion class is nearly the same as in the case of the first analysis conducted. The analysis shows that, while C and P factor are changed, keeping R factor constant, the maximum erosion rate is found to be almost the same as the erosion rate considering all the factors changing overtime in the first analysis. The mean

Table 4

Tabular representation of sediment delivery ratio (SDR), observed and computed sediment yield along the basin for 1981–2000 and 2001–2019, considering the first analysis.

Gauging station	Area (km ²)	Sediment delivery ratio	Observed sediment yield in tons/year		Computed sediment yield in tons/year	
			1981–2000	2001–2019	1981–2000	2001–2019
Andhiyarkore	2.1×10^3	0.076839076	507616.3	207592.6667	281978.7	507707.2
Bamnidih	9.6×10^3	0.063538598	2690081.3	279891.3889	4168963	3251909
Baronda	3.1×10^3	0.073094128	564736.8	363319.0556	753989.1	603947.8
Basantpur	5.8×10^4	0.050734547	11238611.9	4035206	10854604	9339915
Ghatora	2.9×10^3	0.07375947	No Data	710026.1111	846895.9	1306786
Jondhra	2.9×10^4	0.055254032	4252650.9	750625.2222	3713184	791675.6
Kotni	6.9×10^3	0.066264112	No Data	4154052.667	796887.7	6368438
Manendragarh	9.8×10^2	0.084509905	80334.0	849933.3333	366648.1	1496024
Rajim	8.3×10^3	0.064717299	696740	710026.1111	1874181	1306786
Rampur	3.4×10^3	0.072509667	563848.5238	750625.2222	1105717	791675.6
Seorinarayan	4.7×10^4	0.052059476	No Data	4154052.667	7202100	6368438
Simga	1.7×10^4	0.059317467	1830340.571	849933.3333	1703145	1496024

erosion rate and total erosion rate are slightly increased in the second analysis (32.27 tons/ha/yr and 189.46 tons/ha/yr, respectively) with respect to the first analysis (31.89 tons/ha/yr and 187.23 tons/ha/yr, respectively). Around 82.23% of the study region shows a decline in erosion rate with time, as illustrated in Fig. 3. Almost 17.06% of the study area indicates a decrease in erosion rate, particularly in the north and southern parts, with 65.17% of the study area experiencing a drop in the range of $-5-0$ tons $\text{ha}^{-1} \text{yr}^{-1}$. There is a little variation in erosion rate when coupled effects of all the changing factors are compared with the constant rainfall factor on the erosion rate over the years. This explains that change in rainfall, when combined with LULC and NDVI variations, gives quite a similar result when change in rainfall is considered fixed along with changing LULC and NDVI variations. It can be seen from Fig. S4a and S4b in Supplementary Material that with varying decades, there is a shift toward built-up land resulting in less or the same infiltration rate. LULC constituted of more establishments towards 2001–2019 have less P factor value that contributes towards declined erosion rate in the study area. There seems to have a positive correlation between the P factor value and the erosion rate. This outcome is in line with findings from other studies (Wijesundara et al., 2018; Naqvi et al., 2013; Prasannakumar et al., 2012; Jena et al., 2018).

The third analysis shows the impact of changing rainfall on erosion rate. In the third analysis, the maximum mean and total erosion rate are found to be 1.90×10^5 tons $\text{ha}^{-1} \text{yr}^{-1}$, 35.23 tons $\text{ha}^{-1} \text{yr}^{-1}$, 206.83 million tons yr^{-1} . Over here, distinguished change is observed in almost all categorized erosion ranges. Most remarkably, the negligible erosion group ($5-10$ tons $\text{ha}^{-1} \text{yr}^{-1}$) covering around 67.48% of the study region is found to be reduced in terms of the areal extent with respect to the first two analyses.

This explains that while LULC (P factor) is considered to be constant over the years and R factor along with C factor is changed, the erosion rate increases. This current analysis shows that the change in rainfall have more influence on erosion rate rather than other factors.

The change in rainfall and soil loss have a strong correlation between them. A significant increase in rainfall amount is typically followed by the rise in soil erosion (Nigam et al., 2017). While there is a mixed effect of both increase and decrease in erosion rate along with time towards the northern and southern part of the study region in the first and second analysis, there is an inconsiderable increase in erosion rate towards northern and southern parts of the study area during 2001–2019 in the third analysis.

While the first and second analyses show a blended effect of both increase and decrease in erosion rate towards the northern and southern parts of the study region, the third analysis shows an insignificant increase in erosion rate toward the northern and southern parts of the study region from 2001 to 2019 with respect to 1981–2000. In the third analysis, there is a rise in erosion rate with very scanty declines in the middle part of the research area, in contrast to the diverse results in the first and second analyses.

The change in erosion rate is almost the same for the first two analyses for each categorized class. In contrast, in the third analysis, the change in erosion rate is considerably varying from the rest analysis, as shown in Table 3.

Spatial variation of erosivity is noticed in all the analyses and the maximum soil detachment has occurred due to varying rainfall amount. The erosion rate is found to be directly proportional to the rainfall depth in the majority of locations. This finding is also supported by previous studies that established soil erosion is considerably influenced due to differences in rainfall erosivity (Zhang, Liu, 2005; Nearing et al., 2004; Shiono et al., 2013). Increased precipitation intensity is expected to result in increased soil degradation, which has also been concluded by Zhang et al. (2011). This is observed that the change in mean rainfall amount as reflected in R factor affects the erosion rate more than the LULC change. Similarly, de Hipt et al. (2019), (Belay and Mengistu, 2021) and dos Santos et al. (2021) found that the climate change has a larger impact on erosion than LULC.

As anticipated, this study shows that the climate change in terms of change in rainfall and LULC significantly increases spatial variation and becomes the major contributing factor to change in soil erosion rate over the study area.

Despite the major findings gleaned from this study, it is realized that higher spatial resolution satellite data can shed more light on the results of this research. This limitation can be addressed in future studies by collecting sentinel imageries for the assessment. Besides, the use of only one erosion model is a constraint to this study. The use of multi-model approaches could enhance understanding of uncertainty resulting from model choice.

4. Conclusions

The effect of climate change on soil erosion using GIS integrated RUSLE model is investigated in a rainfed basin through analyzing the change in rainfall and LULC. The maximum, mean, and total erosion rates for all the analyses during 2001–2019 were less than during 1981–2000. The maximum erosion rate decreased by 40%, whereas the total and mean erosion rates reduced by 13.85% for 1981–2000 when all the factors (R , C , P) were varied over the years. Whereas with R constant and varying P and C factors, it was observed that there was a 40.38% decrease in maximum erosion rate and 12.83% decrease in total and mean erosion rate with respect to 1981–2000. Similarly, by varying R and C factor and with P factor as constant, it was observed that there was a 26.92% decrease in maximum erosion rate, and 4.84% decrease in mean and total erosion rate.

It was also noticed that the erosion class from 5 to 10 ton $\text{ha}^{-1} \text{yr}^{-1}$ covers 67.4% of the study area during 1981–2000, which elevates to 71.5%, 71.59% and 67.48% during 2001–2019 in the first, second and third analyses, respectively. Thus, it was not the total amount of erosion but the spatial extent of the zone that increased due to changes in the climate.

The model yielded acceptable SDR and SY estimates, and it can be used to predict SY in similar rain-fed basins with sparse data and ungauged basins. Besides, the identified suitable locations and the anticipated changes in the soil erosion risk will help administrators consider soil management measures in erosion-prone sites over the years. In addition, the proposed methods for evaluating the risks of soil loss in a climate change context can be widely applied at the basin scale by performing basin-specific calibration and validation.

CRediT authorship contribution statement

Sushree Sangita Dash: Methodology, Formal analysis, Writing – original draft preparation. **Rajib Maity:** Conceptualization, Methodology, Investigation, Supervision, Funding acquisition, Writing – review & editing.

Declaration of Competing Interest

The authors declare that they have no known competing financial interests or personal relationships that could have appeared to influence the work reported in this paper.

Data availability

Data will be made available on request.

Acknowledgement

The authors are thankful to Food and Agriculture Organization of the United Nations (URL: <http://www.fao.org/soils-portal/data-hub/soil-maps-and-databases/harmonized-world-soil-database-v12/en/> accessed in August 2022) and Central Water Commission (URL: <https://cwc.gov.in/water-year-book-sediment-year-book-water-quality-year-book-meteorological-year-book> accessed in January 2022) for providing the platform to extract the soil map and sediment yield data, respectively for this study. This study is partially supported by the Indian Space Research Organisation (ISRO), Government of India through a sponsored project.

Appendix A. Supporting information

Supplementary data associated with this article can be found in the online version at [doi:10.1016/j.ejrh.2023.101373](https://doi.org/10.1016/j.ejrh.2023.101373).

References

- Allafta, H., Opp, C., 2022. Soil erosion assessment using the RUSLE model, remote sensing, and GIS in the Shatt Al-Arab basin (Iraq-Iran). *Appl. Sci.* 12 (15), 7776. <https://doi.org/10.3390/app12157776>.
- Almohamad, H., 2020. Impact of land cover change due to armed conflicts on soil erosion in the basin of the northern al-kabeer river in syria using the rusle model. *Water (Switz.)* 12, 1–35. <https://doi.org/10.3390/w12123323>.
- Arnoldus, H.M.J., 1980. An approximation of the rainfall factor in the USLE. In: De Boodt, M., Gabriels, D. (Eds.), *Assessment of Erosion*. Wiley, Chichester, England, 127132.
- Asokan, S.M., Dutta, D., 2008. Analysis of water resources in the Mahanadi River Basin, India under projected climate conditions. *Hydrol. Process.: Int. J.* 22 (18), 3589–3603. <https://doi.org/10.1002/hyp.6962>.
- Bagherzadeh, A., Hoseini, A.V., Totmaj, L.H., 2020. The effects of climate change on normalized difference vegetation index (NDVI) in the Northeast of Iran. *Model. Earth Syst. Environ.* 1–13. <https://doi.org/10.1007/s40808-020-00724-x>.
- Behera, M., Sena, D.R., Mandal, U., Kashyap, P.S., Dash, S.S., 2020. Integrated GIS-based RUSLE approach for quantification of potential soil erosion under future climate change scenarios. *Environ. Monit. Assess.* 192 (11), 1–18. <https://doi.org/10.1007/s10661-020-08688-2>.
- Belay, T., Mengistu, D.A., 2021. Impacts of land use/land cover and climate changes on soil erosion in Muga watershed, Upper Blue Nile basin (Abay), Ethiopia. *Ecol. Process.* 10 (1), 1–23. <https://doi.org/10.1186/s13717-021-00339-9>.
- Biswas, S.S., Pani, P., 2015. Estimation of soil erosion using RUSLE and GIS techniques: a case study of Barakar River basin, Jharkhand, India. *Model. Earth Syst. Environ.* 1 (4), 1–13. <https://doi.org/10.1007/s40808-015-0040-3>.
- Borrelli, P., Robinson, D.A., Fleischer, L.R., et al., 2017. An assessment of the global impact of 21st century land use change on soil erosion. *Nat. Commun.* 8, 2013. <https://doi.org/10.1038/s41467-017-02142-7>.
- Borrelli, P., Robinson, D.A., Panagos, P., Lugato, E., Yang, J.E., Alewell, C., Wuepper, D., Montanarella, L., Ballabio, C., 2020. Land use and climate change impacts on global soil erosion by water (2015–2070). *Proc. Natl. Acad. Sci.* 117 (36), 21994–22001. <https://doi.org/10.1073/pnas.2001403117>.
- Chakraborty, R., Pradhan, B., Mondal, P., et al., 2020. The use of RUSLE and GCMS to predict potential soil erosion associated with climate change in a monsoon-dominated region of eastern India. *Arab. J. Geosci.* 13 (20), 1–20073. <https://doi.org/10.1007/s12517-020-06033-y>.
- Chuai, X.W., Huang, X.J., Wang, W.J., Bao, G., 2013. NDVI, temperature and precipitation changes and their relationships with different vegetation types during 1998–2007 in Inner Mongolia, China. *Int. J. Climatol.* 33 (7), 1696–1706. <https://doi.org/10.1002/joc.3543>.
- Cui, L., Shi, J., 2010. Temporal and spatial response of vegetation NDVI to temperature and precipitation in eastern China. *J. Geogr. Sci.* 20 (2), 163–176. <https://doi.org/10.1007/s11442-010-0163-4>.
- Dash, S.S., Paul, J.C., Panigrahi, B., 2021. Assessing soil erosion vulnerability and locating suitable conservation structures for agricultural planning using GIS-a case study of Altuma catchment of Brahmani River Basin, Odisha, India. *Arab. J. Geosci.* 14 (21), 1–15. <https://doi.org/10.1007/s12517-021-08493-2>.
- De Vente, J., Poesen, J., Arabkhedri, M., Verstraeten, G., 2007. The sediment delivery problem revisited. *Prog. Phys. Geogr.* 31 (2), 155–178. <https://doi.org/10.1177/0309133307076485>.
- Doulabian, S., Toosi, A.S., Calbimonte, G.H., Tousi, E.G., Alaghmand, S., 2021. Projected climate change impacts on soil erosion over Iran. *J. Hydrol.* 598, 126432. <https://doi.org/10.1016/j.jhydrol.2021.126432>.
- Durigon, V.L., Carvalho, D.F., Antunes, M.A.H., Oliveira, P.T.S., Fernandes, M.M., 2014. NDVI time series for monitoring RUSLE cover management factor in a tropical watershed. *Int. J. Remote Sens.* 35 (2), 441–453. <https://doi.org/10.1080/01431161.2013.871081>.
- Eekhout, J.P., de Vente, J., 2022. Global impact of climate change on soil erosion and potential for adaptation through soil conservation. *Earth-Sci. Rev.* 226, 103921. <https://doi.org/10.1016/j.earscirev.2022.103921>.
- Eniyew, S., Teshome, M., Sisay, E., Bezabih, T., 2021. Integrating RUSLE model with remote sensing and GIS for evaluation soil erosion in Telkwon Watershed, Northwestern Ethiopia. *Remote Sens. Appl.: Soc. Environ.* 24, 100623. <https://doi.org/10.1016/j.rsase.2021.100623>.
- Gabriels, D., Cornelis, W.M., 2009. Human-induced land degradation. *Land Use Land Cover Soil Sci.* 131–143.

- Gupta, S., Kumar, S., 2017. Simulating climate change impact on soil erosion using RUSLE model— A case study in a watershed of mid-Himalayan landscape. *J. Earth Syst. Sci.* 126 (3), 43. <https://doi.org/10.1007/s12040-017-0823-1>.
- Habtu, W., Jayappa, K.S., 2022. Assessment of soil erosion extent using RUSLE model integrated with GIS and RS: the case of Megech-Dirma watershed, Northwest Ethiopia. *Environ. Monit. Assess.* 194, 318. <https://doi.org/10.1007/s10661-022-09965-y>.
- He, J., Wan, Y.R., Chen, H.T., Wang, S.L., 2022. Effects of land use change on rainfall erosion in Luojiang River Basin, China. *Sustainability* 14 (14), 8441. <https://doi.org/10.3390/su14148441>.
- de Hipt, F.O., Diekkrüger, B., Steup, G., Yira, Y., Hoffmann, T., Rode, M., Näschen, K., 2019. Modeling the effect of land use and climate change on water resources and soil erosion in a tropical West African catchment (Dano, Burkina Faso) using SHETRAN. *Sci. Total Environ.* 653, 431–445. <https://doi.org/10.1016/j.scitotenv.2018.10.351>.
- Houghton, J.T., Ding, Y.D.J.G., Griggs, D.J., Noguier, M., van der Linden, P.J., Dai, X., Maskell, K., Johnson, C.A., 2001. *Climate Change 2001: The Scientific Basis: Contribution of Working Group I to the Third Assessment Report of the Intergovernmental Panel on Climate Change*. Cambridge University Press.
- Huang, C., Zhou, Z., Teng, M., Wu, C., Wang, P., 2020. Effects of climate, land use and land cover changes on soil loss in the Three Gorges Reservoir area, China. *Geogr. Sustain.* 1 (3), 200–208. <https://doi.org/10.1016/j.geosus.2020.08.001>.
- Huang, J., Zhang, J., Zhang, Z., Xu, C.Y., 2013. Spatial and temporal variations in rainfall erosivity during 1960–2005 in the Yangtze River basin. *Stoch. Environ. Res. Risk Assess.* 27 (2), 337–351. <https://doi.org/10.1007/s00477-012-0607-8>.
- IPCC, 2014. In: Mach, K.J., Planton, S., von Stechow, C. (Eds.), *Climate Change 2014: Synthesis Report. Contribution of Working Groups I, II and III to the Fifth Assessment Report of the Intergovernmental Panel on Climate Change*. IPCC, Geneva, Switzerland, pp. 117–130.
- Jena, R.K., Padua, S., Ray, P., Ramachandran, P., Bandyopadhyay, S., Deb Roy, P., 2018. Assessment of soil erosion in subtropical ecosystem of Meghalaya, India using remote sensing and GIS. *Indian J. Soil Conserv.* 46 (3), 273–282. (<http://krishi.icar.gov.in/jspui/handle/123456789/24272>).
- Kabolizadeh, M., Rangzan, K., Mohammadi, S., 2022. Increasing the accuracy of monthly and annual estimates of soil loss in Iran by considering the effect of snow cover in reducing rainfall erosivity. *Arab. J. Geosci.* 15 (15), 1–21. <https://doi.org/10.1007/s12517-022-10592-7>.
- Kavian, A., Alipour, A., Soleimani, K., Gholami, L., Smith, P., Rodrigo-Comino, J., 2019. The increase of rainfall erosivity and initial soil erosion processes due to rainfall acidification. *Hydrol. Process.* 33 (2), 261–270. <https://doi.org/10.1002/HYP.13323>.
- Keesstra, S.D., Bouma, J., Wallinga, J., Tittonell, P., Smith, P., Cerda, A., Montanarella, L., Quinton, J.N., Pachepsky, Y., Van Der Putten, W.H., Bardgett, R.D., 2016. The significance of soils and soil science towards realization of the United Nations Sustainable Development Goals. *Soil* 2 (2), 111–128. <https://doi.org/10.5194/soil-2-111-2016>.
- Khare, D., Mondal, A., Kundu, S., et al., 2017. Climate change impact on soil erosion in the Mandakini River Basin, North India. *Appl. Water Sci.* 7 (5), 2373–2383. <https://doi.org/10.1007/s13201-016-0419-y>.
- Li, Z., Fang, H., 2016. Impacts of climate change on water erosion: a review. *Earth-Sci. Rev.* 163, 94–117. <https://doi.org/10.1016/j.earscirev.2016.10.004>.
- Liu, Q.Q., Xiang, H., Singh, V.P., 2006. A simulation model for unified interrill erosion and rill erosion on hillslopes. *Hydrol. Process.: Int. J.* 20 (3), 469–486. <https://doi.org/10.1002/hyp.5915>.
- Macedo, P.M.S., Oliveira, P.T.S., Antunes, M.A.H., Durigon, V.L., Fidalgo, E.C.C., de Carvalho, D.F., 2021. New approach for obtaining the C-factor of RUSLE considering the seasonal effect of rainfalls on vegetation cover. *Int. Soil Water Conserv. Res.* 9 (2), 207–216. [doi:10.1016/j.iswcr.2020.12.001](https://doi.org/10.1016/j.iswcr.2020.12.001).
- Mahala, A., 2018. Soil erosion estimation using RUSLE and GIS techniques—a study of a plateau fringe region of tropical environment. *Arab. J. Geosci.* 11 (13), 1–18. <https://doi.org/10.1007/s12517-018-3703-3>.
- Martínez-Mena, M., Carrillo-López, E., Boix-Fayos, C., Almagro, M., Franco, N.G., Diaz-Pereira, E., Montoya, I., De Vente, J., 2020. Long-term effectiveness of sustainable land management practices to control runoff, soil erosion, and nutrient loss and the role of rainfall intensity in Mediterranean rainfed agroecosystems. *Catena* 187, 104352. <https://doi.org/10.1016/j.catena.2019.104352>.
- Mitasova, H., Mitas, L., 2001. Multiscale soil erosion simulations for land use management. *Landscape Erosion and Evolution Modeling*. Springer, Boston, MA, pp. 321–347.
- Mondal, A., Khare, D., Kundu, S., Meena, P.K., Mishra, P.K., Shukla, R., 2015. Impact of climate change on future soil erosion in different slope, land use, and soil-type conditions in a part of the Narmada River Basin, India. *J. Hydrol. Eng.* 20 (6), C5014003. [https://doi.org/10.1061/\(ASCE\)JHE.1943-5584.0001065](https://doi.org/10.1061/(ASCE)JHE.1943-5584.0001065).
- Myhre, G., Alterskjær, K., Stjern, C.W., Hodnebrog, Ø., Marelle, L., Samset, B.H., Sillmann, J., Schaller, N., Fischer, E., Schulz, M., Stohl, A., 2019. Frequency of extreme precipitation increases extensively with event rareness under global warming. *Sci. Rep.* 9 (1), 1–10. <https://doi.org/10.1038/s41598-019-52277-4>.
- Naqvi, H.R., Mallick, J., Devi, L.M., Siddiqui, M.A., 2013. Multi-temporal annual soil loss risk mapping employing revised universal soil loss equation (RUSLE) model in Nun Nadi Watershed, Uttarakhand (India). *Arab. J. Geosci.* 6 (10), 4045–4056. <https://doi.org/10.1007/s12517-012-0661-z>.
- Nearing, G.A., Pruski, F.F., O'neal, M.R., 2004. Expected climate change impacts on soil erosion rates: a review. *J. Soil Water Conserv.* 59 (1), 43–50.
- Nigam, G.K., Sahu, R.K., Sinha, M.K., Deng, X., Singh, R.B., Kumar, P., 2017. Field assessment of surface runoff, sediment yield and soil erosion in the opencast mines in Chirimiri area, Chhattisgarh, India. *Phys. Chem. Earth Parts A/B/C.* 101, 137–148. <https://doi.org/10.1016/j.pce.2017.07.001>.
- Ostovari, Y., Ghorbani-Dashkati, S., Bahrami, H.A., Naderi, M., Dematte, J.A.M., 2017. Soil loss estimation using RUSLE model, GIS and remote sensing techniques: a case study from the Dembecha Watershed, Northwestern Ethiopia. *Geoderma Reg.* 11, 28–36. <https://doi.org/10.1016/j.geodrs.2017.06.003>.
- Pal, S.C., Chakraborty, R., 2019. Simulating the impact of climate change on soil erosion in sub-tropical monsoon dominated watershed based on RUSLE, SCS runoff and MIROC5 climatic model. *Adv. Space Res.* 64 (2), 352–377. <https://doi.org/10.1016/j.asr.2019.04.033>.
- Pal, S.C., Chakraborty, R., Roy, P., Chowdhuri, I., Das, B., Saha, A., Shit, M., 2021. Changing climate and land use of 21st century influences soil erosion in India. *Gondwana Res.* 94, 164–185. <https://doi.org/10.1016/j.gr.2021.02.021>.
- Patil, J.P., Sarangi, A., Singh, A.K., Ahmad, T., 2008. Evaluation of modified CN methods for watershed runoff estimation using a GIS-based interface. *Biosyst. Eng.* 100 (1), 137–146. <https://doi.org/10.1016/j.biosystemeng.2008.02.001>.
- Peng, Q., Wang, R., Jiang, Y., Zhang, W., Liu, C., Zhou, L., 2022. Soil erosion in Qilian mountain national park: dynamics and driving mechanisms. *J. Hydrol.: Reg. Stud.* 42, 101144. <https://doi.org/10.1016/j.jehrs.2022.101144>.
- Perović, V., Kadović, R., Djurdjević, V., Braunočić, S., Čakmak, D., Mitrović, M., Pavlović, P., 2019. Effects of changes in climate and land use on soil erosion: a case study of the Vranjska Valley, Serbia. *Reg. Environ. Change* 19 (4), 1035–1046. <https://doi.org/10.1007/s10113-018-1456-x>.
- Pichuka, S., Maity, R., 2017. Spatio-temporal downscaling of projected precipitation in the 21st century: indication of a wetter monsoon over the Upper Mahanadi Basin, India. *Hydrol. Sci. J.* 62 (3), 467–482. <https://doi.org/10.1080/02626667.2016.1241882>.
- Prasannakumar, V., Vijith, H., Abinod, S., Geetha, N.J.G.F., 2012. Estimation of soil erosion risk within a small mountainous sub-watershed in Kerala, India, using revised universal soil loss Eq. (RUSLE) and geo-information technology. *Geosci. Front.* 3 (2), 209–215. <https://doi.org/10.1016/j.gsf.2011.11.003>.
- Rawat, S.S., Nikam, B.R., Kumar, P., Gupta, P.K., 2022. Modeling of sediment yield of tawi catchment to identify the critical sources area. In: Chembolu, V., Dutta, S. (Eds.), *Recent Trends in River Corridor Management. Lecture Notes in Civil Engineering*, vol. 229. Springer, Singapore. https://doi.org/10.1007/978-981-16-9933-7_14.
- Renard, K.G., Foster, G.R., Weesies, G.A., McCool, D.K., Yoder, D.C., 1996. *Predicting soil erosion by water: a guide to conservation planning with the Revised Universal Soil Loss Equation (RUSLE)*. *Agric. Handb.* 703, 25–28.
- dos Santos, J.Y.G., Montenegro, S.M.G.L., da Silva, R.M., Santos, C.A.G., Quinn, N.W., Dantas, A.P.X., Neto, A.R., 2021. Modeling the impacts of future LULC and climate change on runoff and sediment yield in a strategic basin in the Caatinga/Atlantic forest ecotone of Brazil. *Catena* 203, 105308. <https://doi.org/10.1016/j.catena.2021.105308>.
- Shiono, T., Ogawa, S., Miyamoto, T., Kameyama, K., 2013. Expected impacts of climate change on rainfall erosivity of farmlands in Japan. *Ecol. Eng.* 61, 678–689. <https://doi.org/10.1016/j.ecoleng.2013.03.002>.
- Stocking, M.A., Murnaghan, N., 2013. *A Handbook for the Field Assessment of Land Degradation*. Routledge.
- Swanson, K.L., Sugihara, G., Tsonis, A.A., 2009. Long-term natural variability and 20th century climate change. *Proc. Natl. Acad. Sci. U.S.A.* 106 (38), 16120–16123. <https://doi.org/10.1073/pnas.0908699106>.

- Van Rompaey, A.J., Verstraeten, G., Van Oost, K., Govers, G., Poesen, J., 2001. Modelling mean annual sediment yield using a distributed approach. *Earth Surf. Process. Landf.* 26 (11), 1221–1236. <https://doi.org/10.1002/esp.275>.
- Vanoni, V.A., 1975. *Sedimentation engineering. Manuals and Reports on Engineering Practice*. ASCE, USA, p. 745.
- Walling, D.E., 1983. The sediment delivery problem. *J. Hydrol.* 65 (1–3), 209–237. [https://doi.org/10.1016/0022-1694\(83\)90217-2](https://doi.org/10.1016/0022-1694(83)90217-2).
- Wang, R., Chen, J., Chen, X., Wang, Y., 2017. Variability of precipitation extremes and dryness/wetness over the southeast coastal region of China, 1960–2014. *Int. J. Climatol.* 37 (13), 4656–4669. <https://doi.org/10.1002/joc.5113>.
- Wang, R., Gentine, P., Yin, J., Chen, L., Chen, J., Li, L., 2021. Long-term relative decline in evapotranspiration with increasing runoff on fractional land surfaces. *Hydrol. Earth Syst. Sci.* 25 (7), 3805–3818. <https://doi.org/10.5194/hess-25-3805-2021>.
- Wang, R., Li, L., Gentine, P., Zhang, Y., Chen, J., Chen, X., Chen, L., Ning, L., Yuan, L., Lü, G., 2022. Recent increase in the observation-derived land evapotranspiration due to global warming. *Environ. Res. Lett.* 17 (2), 024020 <https://doi.org/10.1088/1748-9326/ac4291>.
- Weesies, G.A., McCool, D.K., Yoder, D.C., 1998. Predicting soil erosion by water: a guide to conservation planning with the Revised universal soil loss equation (RUSLE). *Agric. Handb.* (703).
- Wei, C., Dong, X., Yu, D., Zhang, T., Zhao, W., Ma, Y., Su, B., 2022. Spatio-temporal variations of rainfall erosivity, correlation of climatic indices and influence on human activities in the Huaihe River Basin, China. *Catena* 217, 106486. <https://doi.org/10.1016/j.catena.2022.106486>.
- Wijesundara, N.C., Abeysingha, N.S., Dissanayake, D.M.S.L.B., 2018. GIS-based soil loss estimation using RUSLE model: a case of Kirindi Oya river basin, Sri Lanka. *Model. Earth Syst. Environ.* 4 (1), 251–262. <https://doi.org/10.1007/s40808-018-0419-z>.
- Wischmeier, W.H., Smith, D.D., 1978. Predicting rainfall erosion losses: a guide to conservation planning. *Agriculture handbook*. In: US Department of Agriculture, vol 537. US Government Printing Office, Washington, DC.
- Wu, Y., Chen, J., 2012. Modeling of soil erosion and sediment transport in the East River Basin in southern China. *Sci. Total Environ.* 441, 159–168. <https://doi.org/10.1016/j.scitotenv.2012.09.057>.
- Wuebbles, D.J., 2018. Climate change in the 21st century: looking beyond the Paris agreement. In: Murphy, C., Gardoni, P., McKim, R. (Eds.), *Climate Change and Its Impacts. Climate Change Management*. Springer, Cham. https://doi.org/10.1007/978-3-319-77544-9_2.
- Zhang, G., Xu, X., Zhou, C., Zhang, H., Ouyang, H., 2011. Responses of grassland vegetation to climatic variations on different temporal scales in Hulun Buir Grassland in the past 30 years. *J. Geogr. Sci.* 21 (4), 634–650. <https://doi.org/10.1007/s11442-011-0869-y>.
- Zhang, X.C., Liu, W.Z., 2005. Simulating potential response of hydrology, soil erosion, and crop productivity to climate change in Changwu tableland region on the Loess Plateau of China. *Agric. For. Meteorol.* 131 (3–4), 127–142. <https://doi.org/10.1016/j.agrformet.2005.05.005>.